Probability-matched Reflectivity–Rainfall Relations for a Hurricane from Aircraft Observations

FRANK D. MARKS, JR.
Hurricane Research Division, NOAA/AOML, Miami, Florida

DAVID ATLAS
NASA/Goddard Space Flight Center, Greenbelt, Maryland

PAUL T. WILLIS
Hurricane Research Division, NOAA/AOML, Miami, Florida

(Manuscript received 5 December 1991, in final form 4 December 1992)

ABSTRACT

The probability-matching method (PMM) was used to determine the relation between the distribution of equivalent reflectivity Z_e measured by an airborne C-band radar and that for concurrently measured rain rate R by a disdrometer on the same aircraft in the eyewall and outer bands of Hurricane Anita in 1977. When the PMM is applied to the disdrometer population of Z's and R's one finds that the Z–R relations differ significantly from those obtained by linear regression of their logarithms. Such regression relations are deceptive. When PMM is applied to the set of Z_e's and R's we get a family of Z_e–R relations as a function of range which differ significantly from the traditional disdrometer-based Z–R relation for hurricanes by Jorgensen and Willis (JW). These new relations are approximate power laws with slope (exponent) which decrease with increasing range. At ranges less than about 35 km the reflectivity in the eyewall exceeds that in the outer bands and is consistent with the expectation from the disdrometer-based relations. At greater ranges the converse is true due to beamwidth averaging over a broader beam and different vertical profiles of reflectivity in the eyewall and outer bands. We also devise a method to obtain an "effective zero-range" Z_e–R relation. This differs from the JW relation by −8.2 dBZ and reflects an error in the radar calibration. This approach is a novel way to calibrate an airborne meteorological radar. The methods may be used with any type of rainstorms and provide a means of using airborne radar and disdrometer systems for air-truthing rainfall measurements from space.

1. Introduction

This work is aimed at the determination of the relationship between the effective reflectivity factor Z_e as measured by the radar and rain rate R for hurricanes as observed by an airborne radar and to establish basic airborne radar methods of estimating rainfall over the oceans and other areas inaccessible to ground-based radar and raingages. It is an extension of the approaches of Calheiros and Zawadski (1987), Atlas et al. (1990a), and Rosenfeld et al. (1993), in which a relationship between Z_e and R is determined by a probability-matching method (PMM).

The method finds the set of pairs of Z_{e_i} and R_i at which the absolute cumulative probabilities of the two are equal, where i represents the ith percentile of the distribution. In all previous studies the radar observations were made by ground-based radars and the rain rates were determined by raingages. In the present case, however, we match the probability density functions (PDF) of radar-measured Z_e, using an airborne radar, to that of R as measured by a Knollenberg Particle Measurement Systems (PMS) optical array spectrometer probe (hereafter referred to as PMS probe or disdrometer) on the same aircraft.

The essential differences between the PMM scheme and the traditional method of using a disdrometer-based Z–R relation are twofold: 1) PMM uses reflectivities as measured by the radar rather than those computed from drop size distributions. It therefore incorporates all the effects that the beam and the propagation medium exert on the reflectivity; and 2) the matched Z_e–R relation assures that the PDF of R retrieved from its application will mimic the actual PDF of R provided that the sample of Z_e is representative of the population. Moreover, in order to be representative, one generally requires a sufficiently large space–time sampling domain. Such sampling is more appropriate to climatological and hydrological measurements

Corresponding author address: Dr. Frank D. Marks, Hurricane Research Division, NOAA/AOML, 4301 Rickenbacker Causeway, Miami, FL 33149-1097.

than to those at a point in space or time. While the traditional Z–R relations are frequently applied to such point measurements it is well known that such observations are fraught with problems (Austin 1987; Joss and Waldvogel 1990). In this work we also treat the eyewall and the outer bands separately. An important by-product is a method to calibrate an airborne radar.

2. Approach

The essence of the probability-matching method is best presented in the most recent work by Rosenfeld et al. (1990, 1993, hereafter RWA). For our purposes it will help to clarify some of the key definitions and approaches in the prior work. For example, the absolute or unconditional PDF of rain rate R refers to the entire time–space domain and includes both rainy and nonrainy periods and areas. On the other hand, the conditional PDF refers only to the rainy periods and regions. The absolute PDF is thus the sum of the conditional PDF plus a dirac delta function at $R = 0$ corresponding to the fraction of the domain in which no rain occurs, normalized to unit area.

Calheiros and Zawadzki (1987) and RWA emphasize the importance of matching the absolute PDFs of Z_e and R in order to guarantee that the radar reflectivity above some threshold actually corresponds to rain. In the PMM one finds the set of pairs of Z_{e_i}, R_i at which the absolute cumulative probabilities of the two are equal, where i represents the ith percentile of the cumulative density function (CDF).

In order to be sure that the radar observations represent the actual frequency and areal extent of rain, RWA compared radar and rain events that were collocated in time and space. This was done by selecting a group of radar pixels centered around each raingage location to determine the threshold Z_0 aloft which produced the same number of rain events as determined by the threshold rain rate of the gages at the surface. This is a reminder that the threshold rate R_0 of the raingage or disdrometer becomes the defining boundary between rain and no rain. Also, because the radar beam distorts the true structure of the storm as a result of beamwidth weighting and sidelobes, the value of Z_0 varied with range from the radar and with storm type. It was then possible to obtain matched pairs of Z_{e_i} and R_i by accumulating the frequency of occurrence of Z_e above the threshold Z_0. This assures that (a) the frequency of rain events seen by the radar in each range interval equals the frequency of rain events observed by the gauge or disdrometer; and (b) all radar pixels with $Z_e < Z_0$ (e.g., those due to beamwidth spreading) compose the portion of the absolute PDF at $R < R_0$, the level below which there is no measurable rain.

With the airborne radar and disdrometer, however, this procedure is not necessary because the disdrometer on board the aircraft is effectively "collocated" with the radar observations along the aircraft heading within 90 min for radar ranges less than 150 km. Also, with the exception of a relatively few points within the hurricane eyewall, there were no echoes that occurred with no measurable rain. In other words, Z_0 corresponds to the minimum detectable reflectivity of the radar. While the threshold Z_0 varies with range, we simply match that threshold to the constant R_0 threshold of the disdrometer. In short the effective collocation of the radar and disdrometer data provided by the moving platform, and the equality of Z_0 to the minimum radar reflectivity permits the simultaneous determination of the conditional and unconditional PDFs.

3. Data

The observations were made on board the NOAA WP-3D in Hurricane Anita between 0038 and 0730 UTC 1 September 1977. We deal only with the data taken at a flight level of 3.1 km in order to be entirely in the rain. The 0°C level was at a height of 4.5 km.

The R dataset is composed of 1261 10-s samples, or approximately 3.5 h of data. Figure 1 shows the distribution of the 10-s samples around the storm. The samples cover all the major precipitation features of the storm (eyewall and rainbands) in each quadrant. However, there was a tendency to oversample the eyewall region. Roughly 10% of the R samples were in the eyewall region, which covers only 5% of the area within a 120-km radius from the storm center.

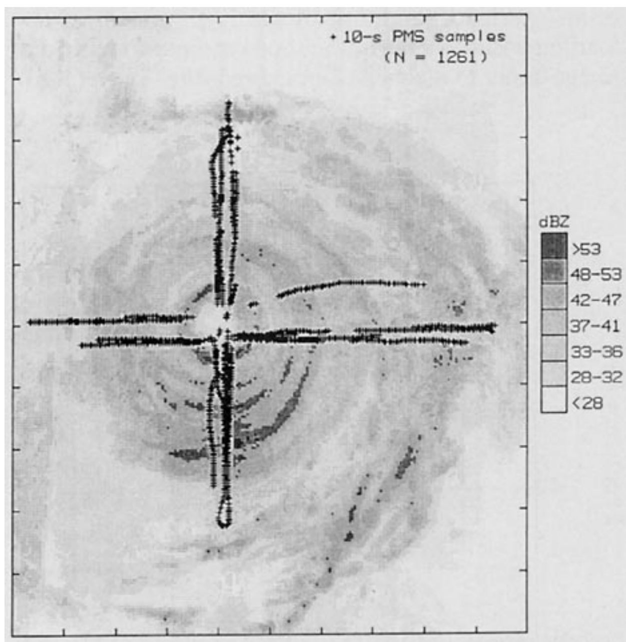

FIG. 1. Lower-fuselage radar time composite for 0327–0536 UTC 2 September 1977 at 3-km altitude. Reflectivity (dBZ) is denoted by increasing shades of gray. The domain is 300 km × 360 km. Tick marks are separated by 30 km in the x direction and 36 km in the y direction. The location of each 10-s rainfall-rate sample for the whole dataset is denoted by "+."

The R values are adjusted to surface estimates by applying a density (ρ) correction from an altitude of 3.1 km ($\rho = 0.861 \times 10^{-3}$ gm^{-3}) to the surface ($\rho_0 = 1.20 \times 10^{-3}$ gm^{-3}). The correction, $(\rho_0/\rho)^{0.5} = 1.18$, increases the R estimates by about 20% over those at flight level.

The PDFs of R are computed from measurements made with the 2D-P PMS probe. The data are the same as those gathered by Jorgensen and Willis (1982) (hereafter JW) except that we separated them by eyewall and outer rainbands. Each rain sample corresponds to 10 s of data or 1.25 km along the track and a total sample volume of 2 m^3. Each PDF is stored in 1-dBR bins; that is, 10 log$R$ where the log is taken with respect to 1 mm h^{-1}.

Raw number distributions of particles are obtained from shadow images of the droplets. These values are converted to numbers per cubic meter by dividing by the sample volume, which is computed as in Heymsfield and Parrish (1978) as the product of the sampling area, the true airspeed, and the sampling time. The sampling area is the product of the depth of field and the effective array width. The depth of field as a function of the number of diodes occluded was provided as part of the probe calibrations by the manufacturer. The effective array width is 6.2 mm, based on the criterion of only sizing particles that have their centers in the viewing area. The true airspeed comes from the flight-level data system.

The sampling period is nominally 10 s. However, the actual sampling time may be less than 10 s because of an overload condition of the PMS system. Overloading arises whenever the time required to write one image buffer to magnetic tape exceeds the time required to fill the other buffer with new image data. The time the PMS system does not sample any particles is expressed as the overload percent. Typical overload percentages for hurricane flights with the precipitation probe are 0%–15% in the stratiform rain areas and 30%–50% in convective clouds. Hence, while a normal 10-s sample has a typical sample volume of 2 m^3, when there are numerous particles and the overload percentage is high, the sample volume decreases proportional to the fraction of time the probes are overloaded. For example, if the overload percent is 75%, then the sample volume is one quarter of that for a full 10-s sample.

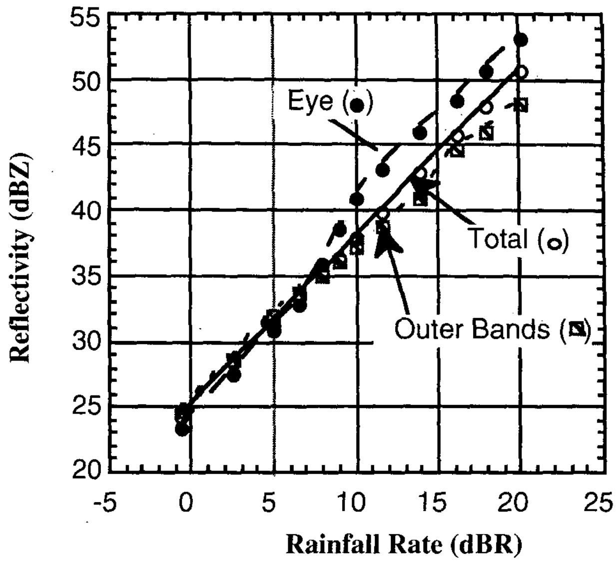

FIG. 3. The Z–R functions obtained by the PMM applied to the PMS data in the eyewall (dashed), the outer bands (small dash), and the total (solid).

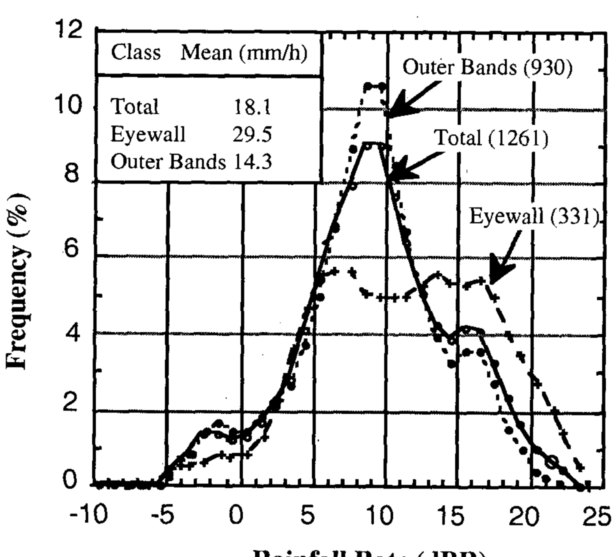

FIG. 2. PDFs of R (dBR) for the eyewall (dashed, +), the outer bands (dotted, filled circle), and the total (solid, open circle). Numbers in parentheses are the number of samples.

The 10-s sampling period is generally sufficient to allow between 500 and 800 drops to be included in the sample; however, as pointed out by Cornford (1968), severe sampling problems can exist at the large end of the spectra (3–6 mm), because drop densities are too low to allow for more than 10–20 drops in these categories. The 10-s sampling time was chosen as a compromise between sample volume and data homogeneity; that is, 10 s represents 1.0–1.6 km of flight distance.

Another potential source of error is incorrectly sizing particles as big as the effective array width (6.2 mm). An examination of individual drop images (not shown here) reveals very few drops larger than 4 mm in diameter. Hence, this problem is minimized.

Figure 2 shows the PDFs of R for the outer bands (930 samples with mean of 14.3 mm h^{-1}), the eyewall (331 samples with mean of 29.5 mm h^{-1}), and the combination with mean of 18.1 mm h^{-1}. The eyewall PDF is essentially flat over the range of 6–17 dBR (4–50 mm h^{-1})—reflecting the asymmetry between intense rain which occurs in one sector of the eyewall and the weaker rates which mark the stratiform regions of the eyewall. The outer band PDF is rather narrow. Nevertheless, all three can be fitted roughly by lognormal distributions.

We have used the PMS rain data to obtain regression relations for the eyewall and the outer bands and use the function found by JW for the total sample. These are as follows: eyewall—$253R^{1.32}$; outer bands—$341R^{1.25}$; total—$311R^{1.27}$. According to these relations, the ratio of reflectivity in the outer bands to that in the eyewall is about 1.35 (or 1.3 dBZ) for the same rain rate. In order to obtain a more realistic picture we have applied the PMM to the set of Z's and R's computed from the PMS rain data. The results are shown in Fig. 3. There we see that at rates less than 8 dBR (6.3 mm h^{-1}) the reflectivities are equal in the eye and outer bands; but at rates greater than 10 dBR (10 mm h^{-1}), Z in the eye is 3.5–5 dBZ greater than that in the outer bands. This is more in line with expectation since the drops in the eyewall tend to be larger on average than those in the outer bands. Figure 3 thus indicates that simple regression relations over the entire range of the Z and R domain measured by a disdrometer are deceptive and that the true relations are not necessarily power laws.

The PDFs of Z_e are taken from the C-band lower-fuselage (LF) radar data from the same flight. The radar has horizontal and vertical beamwidths of 1.1° and 4.1°, respectively, antenna gain of 40 dB, wavelength of 5.59 cm, a pulse width of 6 μs, and minimum detectable signal of −100 dBm. The Z_e dataset is collected from 1-km × 1-km Cartesian bins, interpolated from the raw polar data for each sweep to the position of each 10-s R sample along the flight track of the aircraft within 450 s (~60 km) of the time of each radar sweep (Fig. 1). The PDFs are stored at 1-dBZ resolution and are stratified in 10 km annuli of range out to a maximum of 120 km from the aircraft. Table 1 contains of the PDF of Z_e for selected range intervals.

Figure 4 shows a composite plot of the ten cumulative density functions (CDFs) corresponding to the outer-band region out to a range of 100 km. For example, the CDF of Z_e between 90 and 100 km is given by the set of points in a vertical column plotted at a range of 95 km where each point corresponds to the percentile shown by the coded legend. We then obtained the best fit isopleth to each ith percentile as a function of range. This was done to eliminate the statistical noise due to sampling and the artifacts in the CDFs due to anomalous echoes detected via the sidelobes of the beam.

The threshold R was set to 0.5 mm h^{-1} (−3 dBR), which left out 6.5% of the rain rates sampled by area over the total sample (6.7% for the outer bands and 6.03% for the eyewall), but only 0.1% of the rain sampled by volume (0.15% for the outer bands and 0.05% for the eyewall). Reflectivity data were included only if there was a corresponding R value above the threshold R_0. This R threshold corresponded closely to the minimum detectable signal for the PDF of Z_e in the 0–10-km range interval (−4 dBZ). As range increased, the threshold R corresponded to higher Z_e values because of the range-dependence of the minimum detectable signal. Hence, the effective threshold Z_e was the minimum detectable signal of the area-weighted mean range for each 10-km annulus.

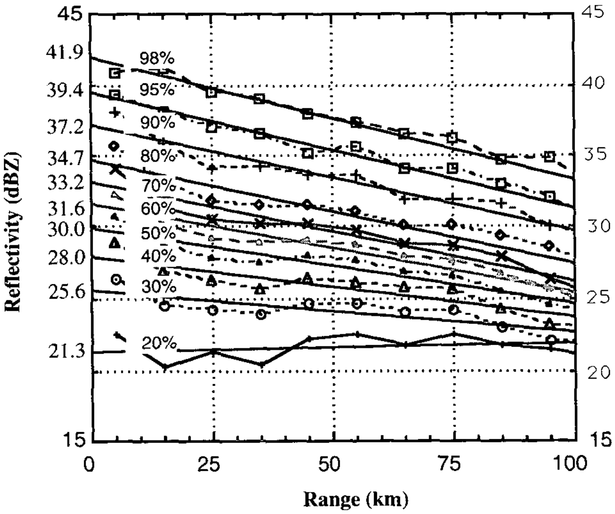

FIG. 4. Curves of constant cumulative percentiles of radar-measured Z_e as a function of range for the outer bands. Percentiles are as shown by the legend. Solid straight lines are best-fit regressions to the data. Numbers adjacent to the left vertical axis are the Z_e values obtained when the smoothed percentile curves are extrapolated to zero range; these comprise the zero-range CDF.

4. Results

The principal features of the CDFs of Z_e seen in Table 1 and Fig. 4 are 1) the decrease in the median Z_e; and 2) the narrowing of the distribution with increasing range. The main cause for the narrowing is the increase in the minimum detectable signal with increasing range, accompanied by a decrease in the maximum Z_e values due to averaging by an increasingly broad beam and by rainfall attenuation. Indeed, all the moments of the PDFs of Z_e decrease with increasing range as well.

Because of the erratic nature of the CDFs of Z_e at the short ranges, we have extrapolated the best-fit isopleths of the percentiles to zero range. This gives us an "effective zero-range CDF of Z_e," which is equivalent to what we would expect to measure with an infinitely narrow beam. The "zero-range" Z_e values are plotted along the left-hand vertical axis in Fig. 4. We then used the PMM to match the latter CDF to that of R and obtain the "zero-range Z_e–R relation." This was done for the eyewall, the outer bands, and the combination. The results are shown in Fig. 5 where we also plot the disdrometer-based Z–R relation of JW for the entire storm; that is, $Z = 311R^{1.27}$.

We see that the zero-range relations are not significantly different from power laws. More importantly, however, the relation for the total sample falls an average of 8.2 dBZ below the JW relation. Since the latter is what we should measure with an infinitely narrow beam, it is clear that the radar was miscalibrated.

The LF radar receiver was calibrated at the beginning and the end of the hurricane season, roughly one month before and two months after the Anita dataset was collected. The receiver calibration done at the end of the season was much different from that done at the beginning of the season (used for the Anita dataset), suggesting that the receiver had drifted or had been retuned. Neither calibration produced a Z_e distribution comparable to that from the disdrometer data reported by JW. It is impossible to determine the correct receiver calibration to use for this dataset at this time.

The 8.2-dB underestimate of the reflectivities indicated in Fig. 5 is consistent with anecdotal reports about the discrepancy between the airborne and ground-based radar rainfall estimates. However, it should be noted that this large underestimate is not typical. In a comparison of LF-derived Z_e distributions with land-based radar and PMS disdrometer distributions in a Winter MONEX (Monsoon Experiment) convective system, Houze et al. (1981) showed that the two radar estimates agreed to within 1–2 dB, while those from the disdrometer and LF radar differed by 2–3 dB. In any case, the comparison of the zero-range extrapolated Z_e–R relation based upon the PMM to that of the disdrometer Z–R relation is a unique method to calibrate an airborne meteorological radar.

Figure 6 shows the Z_e–R relations for the outer bands at three range annuli, and for the eyewall at only 40–50 km. These are based upon the unsmoothed CDFs shown in Fig. 4, and they are corrected for the −8.2-dBZ calibration error. Note that the relation for 80–90 km has a smaller slope than that for 40–50 km. This is due to the fact that the median and slope of the CDF of R remain constant with range while the median and slope of the CDF of Z_e both decrease with range. In other words, the breadth of the PDF of Z_e decreases with range while that of R is independent of range. Thus the breadth of Z_e values that matches the breadth of R values decreases with range, thereby decreasing the slope of the resultant Z_e–R relation.

Also, while the disdrometer-based Z–R relations in Fig. 3 show that the eyewall reflectivity at rain rates greater than about 8.2 dBR exceed those in the outer bands, Fig. 6 indicates that the converse is true at all rates at 40–50 km. This is due to beamwidth averaging over a different vertical reflectivity profile in the eyewall than in the outer bands; the effect will be demonstrated further below.

In the inset to Fig. 6 we present the power-law regression relations which best fit the data. It is not too surprising that power laws are quite good since one can approximate the PDFs of R (see Fig. 3) and of Z_e by

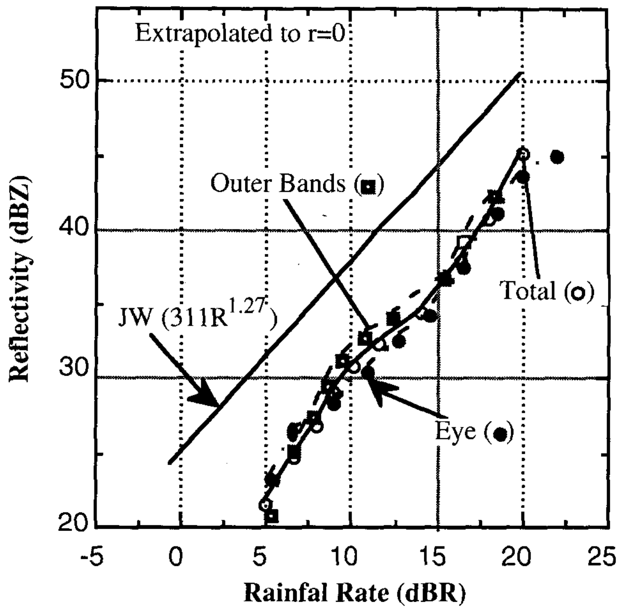

FIG. 5. The PMM Z_e–R relations for "effective zero range" for the outer bands (dash), the eyewall (dot), and the total (solid) as compared to the disdrometer-based Z–R relation of Jorgensen and Willis (1982) for the entire storm.

lognormal distributions. Under these conditions Atlas et al. (1990b) have noted that the Z_e–R relations are forced to be power laws.

In Fig. 7 we plot the mean measured reflectivity for both the outer bands (solid curve) and the eyewall (dashed curve) as a function of range. We see that at ranges less than 35 km, the eyewall Z_e's exceed those in the outer bands. However, the converse is true at greater ranges. Note that the short-range behavior is consistent with the finding from the disdrometer data in Fig. 3 that at rain rates in excess of 8 dBR, the eyewall Z_e's exceed those in the outer bands. This result is expected since as range approaches zero, the radar Z_e–R relation should approach that of the disdrometer.

On average, the drops in the eyewall are larger than those in the outer bands, thus producing larger Z_e's. On the other hand, at greater ranges, Z_e is determined more by the convolution of the beam with the vertical reflectivity profile and by the effects of attenuation. In particular, we note that the wide vertical beam of the LF radar averages over a significant depth of the vertical profile of Z which, except for the bright band, decreases monotonically with height (Szoke et al. 1986). The result of unequal beam illumination, as shown by Marks (1985) (cf. Fig. 16) for the airborne radars and Burpee and Black (1989) (cf. Fig. A1) for the WSR-57 radar, is a slight increase in signal at midranges (~40–100 km) where the beam is centered on the bright band. The outer band curve in Fig. 7 is slightly higher than that for the eyewall in the 40–100-km range because the outer-band region contains more extensive brightband areas than the eyewall. Otherwise, the outer-band curve would drop off in a similar manner to the eyewall curve.

It is important to note that all the exponents of the best-fit Z_e–R power laws shown in Fig. 7 are smaller than the exponent determined from the disdrometer data. This fact has been explained above and serves to emphasize the fact that one cannot use a disdrometer-based Z–R relation to retrieve radar-measured rain rates except at the very short ranges. Unfortunately, this practice is still widespread.

Finally, we need to consider the effects of vertical air motions. These may have a significant impact on the Z_e–R relations determined above. In counting the drops measured by the 2D-P probe no distinction was made between those drops that were rising or falling. Obviously, in a significant updraft, a substantial portion of the rain may be rising. Since the precipitation rate is given by

$$R = \sum m_i v_i = v_m M,$$

where the summation is taken over the product of the mass m_i and terminal fallspeed v_i of the particle size distribution per unit volume, and v_m is the mass-weighted fallspeed, and M is the total mass. Thus, drafts will alter R by the ratio $(v_m + w)/v_m$ where the sign is positive for upward motion. Thus if $w = +0.1|v_m|$ then R will be in error by -10% and of opposite sign for a downdraft.

Since no allowance is made for drafts in the PMM scheme we refer to the resulting R as the "equivalent zero-draft rain rate." Following Kessler (1969), Lee (1988) has argued that the rates measured by a gauge at a point on the surface from a rain falling in a draft aloft will be unaffected by the draft because the change in the mass-weighted fallspeed will be compensated exactly by the convergence. However, he notes that the updraft-associated convergence (downdraft divergence) will cause the rain to be spread over a smaller (larger) area at the surface than it occupied aloft, thus resulting in an erroneous estimate of the areawide rainfall.

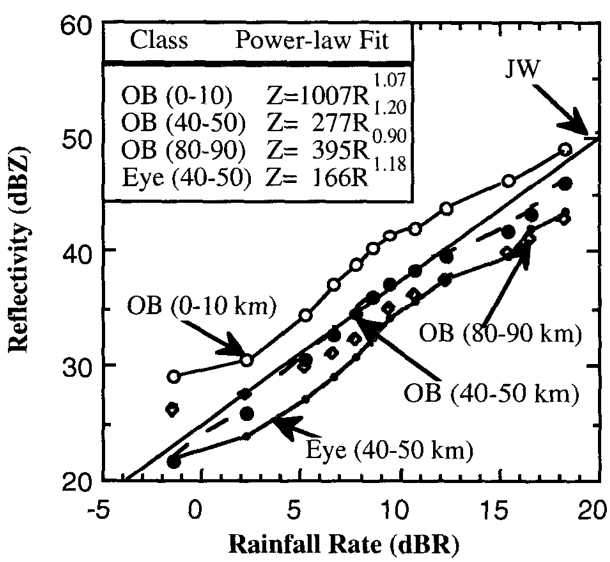

FIG. 6. Matched Z_e–R functions for range intervals, r = 0–10 (open circle), 40–50 (filled circle), and 80–90 km (diamonds) for the outer bands and that for the eyewall at 40–50 km (dots). The curves are corrected for the −8.2-dBZ error. The inset table shows the corresponding power-law fits for the corrected Z_e–R functions.

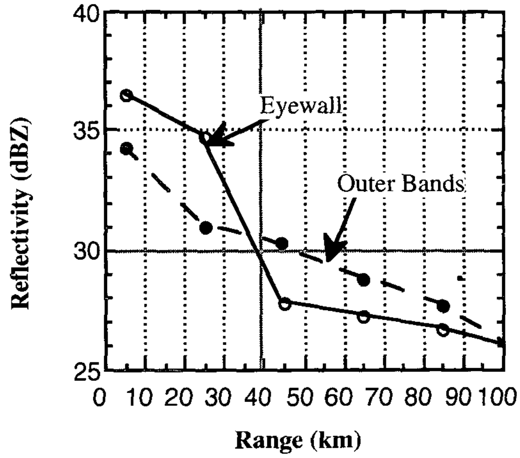

FIG. 7. Variation of the mean Z_e with range for the outer bands (solid) and the eyewall (dashed).

Lee also mentions situations in which either all or a portion of the precipitation rises to be carried away and fall out elsewhere, and the effects of shear in spreading the rain at the surface. Barring effects of growth and evaporation, however, he correctly notes that the product of M times the area must remain constant. More specifically, the raindrop spectrum will be sorted first by the up- and downdrafts, and then by the wind shear. The total rain mass will then be partitioned into elements which follow different trajectories in time and space, thereby reaching the ground at a variety of places and times. However, the sum of these elements of mass must equal that found at the time and place of initial observation (barring growth or evaporation). The result is that the rain rates deduced from reflectivity measurements are not necessarily representative of the instantaneous rates at observation time but, except for the losses which may be incurred by outflow in the anvil, they are a measure of what will ultimately fall out over the region crossed by the storm.

In the case of a hurricane, the "equivalent zero-draft rain rate" at any level (i.e., 3.1-km level in Anita) will ultimately reach the surface over a substantially different area than was occupied aloft. No gain or loss due to growth or evaporation along the particle trajectories is assumed. Marks and Houze (1987), using computed particle trajectories in the eyewall region of Hurricane Norbert, showed that while the eyewall is marked by substantial updrafts, the hydrometeors that are rising in the updraft either fall out in the eyewall ring counterclockwise from where they were observed, or in the case of the smaller particles, rise to form the anticyclonic outflow anvil region near the storm top. Atlas et al. (1963) first deduced this type of particle sorting in the outer bands.

In hurricanes, the drafts in the outer rainbands are rather modest (Jorgensen et al. 1985). Only the strongest 10% of the up- and downdraft cores (i.e., those exceeding 1 m s^{-1} over a distance of 500 m) reach 3 m s^{-1}, and these occupy only 5%–10% of the total area. This is in accord with the work of Marks (1985) in which he reports that less than 5% of hurricane areas contain echoes in excess of 40 dBZ. Similar conclusions were reached by Malkus et al. (1961) based upon a study of radar and cloud photography of Hurricane Daisy (1958). It is only in the eyewall that Jorgensen et al. (1985) report that the updraft cores at 3 km in altitude reach 5 m s^{-1} and cover about 55%–60% of the area of the 5-km annulus inside the ring of maximum wind speed.

Hence, the Z_e–R relations reported here will provide good estimates of the rain reaching the surface in the outer bands. However, the Z_e–R relations for the eyewall apply only to the "equivalent zero-draft rain rates" and provide only an estimate of the rain flux at observation time. Only when averaged over time and space will the total rain volume emanating from the eyewall equal that which would have come from these zero-draft rates.

5. Conclusions

The PDF of rain rate R is much narrower in the outer rainbands of Hurricane Anita than in the eyewall. The mean rain rates are also much smaller. The PDFs may be approximated roughly by log-normal distributions.

The conventional power-law Z–R regression relations based upon scatterplots of disdrometer measurements are misleading in Hurricane Anita. The use of the PMM provides more realistic relations which show higher eyewall reflectivities for the same rain rates at rates in excess of 8 dBR (6.3 mm h^{-1}).

We have determined the PDFs of radar-measured reflectivity Z_e in each 10-km range annulus and smoothed them in range to eliminate sampling noise and radar artifacts. The smoothed PDFs are then extrapolated to zero range. The zero-range PDF of Z_e is then matched to that of R by PMM to provide an effective zero-range Z_e–R relation. Comparison of the latter to the disdrometer-based Z–R relation of Jorgensen and Willis (1982) shows that the radar reflectivities are 8.2-dBZ low, pointing to a serious long-term error in the radar calibration. This approach provides a unique method of calibrating an airborne meteorological radar.

After correction for the 8.2-dBZ error, the PMM provides a set of Z_e–R relations for each range annulus. These are approximate power laws with slopes (exponents) that decrease with range due to the decreasing breadth of the PDFs of Z_e that are matched to the constant breadth of the PDF of R. This is characteristic of all relations between radar-measured reflectivity and rain rate and serves to emphasize the point that disdrometer-based relationships are not applicable to rain retrievals except at the very shortest ranges.

At ranges less than about 35 km the mean radar-measured Z_e in the eyewall exceeds that in the outer bands in accordance with expectations at the short ranges and with the different vertical Z profiles in the eyewall and the outer bands.

Wherever the vertical drafts become a significant fraction of the mass-weighted mean fallspeed of the drop size distribution, the Z_e–R relations will not provide good estimates of the rain rates at the surface. Accordingly we refer to the corresponding R's as the "equivalent zero-draft rain rates." The presence of drafts will cause the rain to be spread out over a different space–time domain than that at the time and place observed. However, barring growth or evaporation, the total rain volume that ultimately reaches the surface will be correct. It is mainly in the eyewall where this is a serious problem.

The methods used here are directly applicable to other types of rainstorms in areas that are inaccessible to ground-based radar and rainfall measurements. In particular, they provide a means of obtaining the Z_e–R functions for such rains. They also demonstrate the utility of the airborne system for purposes of calibrating and validating observations from space.

Acknowledgments. We thank Dr. Stanley Rosenthal for encouraging us to pursue this study. We also appreciate the stimulating suggestions of Dr. Daniel Rosenfeld of Hebrew University. Support for David Atlas was partially provided by the Hurricane Research Division through the Cooperative Institute for Marine and Atmospheric Studies, University of Miami, and NASA. Joyce Berkeley, Robert Black, Neal Dorst, and Nancy Griffin were instrumental in the development of the rainfall and reflectivity datasets. We thank the crews and engineers of NOAA's Aircraft Operations Center for their operation and maintenance of the radar and cloud physics instruments during hurricane research flights.

REFERENCES

Atlas, D., D. Rosenfeld, and D. A. Short, 1990a: The estimation of convective rainfall by area integrals. Part I: Theoretical and empirical basis. *J. Geophys. Res.*, **95**, 2153–2160.

——, ——, and D. B. Wolff, 1990b: Climatologically tuned reflectivity–rain rate relations and their implications for area time integrals. *J. Appl. Meteor.*, **29**, 1120–1139.

——, K. R. Hardy, R. Wexler, and R. Boucher, 1963: The origin of hurricane spiral bands. *Geofis. Int.*, **3**, 123–132.

Austin, P. M., 1987: Relation between measured radar reflectivity and surface rainfall. *Mon. Wea. Rev.*, **115**, 1053–1070.

Burpee, R. W., and M. L. Black, 1989: Temporal and spatial variations

of rainfall near the centers of two tropical cyclones. *Mon. Wea. Rev.,* **117,** 2204–2218.
Calheiros, R. V., and I. Zawadski, 1987: Reflectivity–rain rate relationships for radar hydrology in Brazil. *J. Climate and Appl. Meteor.,* **26,** 118–132.
Cornford, S. G., 1968: Sampling errors in measurements of particle size distributions. *Meteor. Mag.,* **97,** 12–16.
Heymsfield, A. J., and J. L. Parrish, 1978: A computational technique for increasing the effective sampling volume of the PMS two-dimensional particle size spectrometer. *J. Appl. Meteor.,* **17,** 1566–1572.
Houze, R. A., Jr., S. G. Geotis, F. D. Marks, Jr., D. D. Churchill, and P. H. Herzegh, 1981: Comparison of airborne and land-based radar measurements of precipitation during winter MONEX. *J. Appl. Meteor.,* **20,** 772–783.
Jorgensen, D. P., and P. T. Willis, 1982: A *Z–R* relationship for hurricanes. *J. Appl. Meteor.,* **21,** 356–366.
——, E. J. Zipser, and M. A. LeMone, 1985: Vertical motions in intense hurricanes. *J. Atmos. Sci.,* **42,** 839–856.
Joss, J., and A. Waldvogel, 1990: Precipitation measurement hydrology. *Radar in Meteorology,* David Atlas, Ed., Amer. Meteor. Soc., 577–606.
Kessler, E., 1969: On the distribution and continuity of water substance in the atmospheric circulation. *Meteor. Monogr.,* No. 40, Amer. Meteor. Soc., 84 pp.
Lee, A. C. L., 1988: The influence of vertical air velocity on the remote microwave measurement of rain. *J. Atmos. Oceanic Technol.,* **5,** 727–735.
Malkus, J. S., C. Ronne, and M. Chaffee, 1961: Cloud patterns in Hurricane Daisy. *Tellus,* **13,** 8–30.
Marks, F. D., Jr., 1985: Evolution of the structure of precipitation in Hurricane Allen (1980). *Mon. Wea. Rev.,* **113,** 909–930.
——, and R. A. Houze, 1987: Inner core structure of Hurricane Alicia from airborne Doppler radar observations. *J. Atmos. Sci.,* **44,** 1296–1317.
Rosenfeld, D., D. Atlas, and D. A. Short, 1990: The estimation of convective rainfall by area integrals. Part II: The height area rainfall threshold (HART) method. *J. Geophys. Res.,* **95,** 2161–2176.
——, D. B. Wolff, and D. Atlas, 1993: General probability relations between radar reflectivity and rain rate. *J. Appl. Meteor.,* **32,** 50–72.
Szoke, E. J., E. J. Zipser, and D. P. Jorgensen, 1986: A radar study of convective cells in GATE. Part I: Vertical profile statistics and comparison with hurricane cells. *J. Atmos. Sci.,* **43,** 182–197.